Physica E 44 (2011) 506–510

Contents lists available at SciVerse ScienceDirect

Physica E

journal homepage: www.elsevier.com/locate/physe

Synthesis of copper oxide nanostructures via a composite-Hydroxide-mediated approach: Morphology control and the electrochemical performances as anode material for lithium ion batteries

Minwei Xu, Fei Wang *, Mingshu Zhao, Sen Yang, Zhanbo Sun, Xiaoping Song *,[1]

MOE Key Laboratory for Nonequilibrium Synthesis and Modulation of Condensed Matter, School of Science, Xi'an Jiaotong University, Xi'an 710049, PR China

ARTICLE INFO

Article history:
Received 26 January 2011
Received in revised form
26 August 2011
Accepted 28 September 2011
Available online 6 October 2011

ABSTRACT

Various CuO nanostructures with different morphologies, such as nanosheets, nanowires and nanobundles have been synthesized via a composite-hydroxide-mediated approach. The morphologies can be easily tailored by adjusting the concentration of precursor and the possible morphology transformation process is proposed. Scanning electron microscopy, X-ray diffraction and galvanostatical charge–discharge test are employed to characterize the morphology, structure and electrochemical properties of the CuO nanostructures, respectively. It is found that different morphologies of CuO result in different electrochemical performances. Compared to others, CuO nanosheets exhibit not only high reversible capacity but also good cycling stability. The improved electrochemical performance is attributed to the novel 3D hierarchical nanostructure, which could relieve the stress caused by the drastic volume change and ensure good capacity retention.

1. Introduction

As an important p-type semiconductor with a narrow band gap of 1.2 eV, cupric oxide (CuO) has been extensively studied owing to its potential applications in sensors, high critical temperature superconductors, field emission emitters, catalysts, etc. [1–8]. Also, CuO is a promising anode material for lithium ion batteries [9,10], which attracts considerable attention due to its advantages of high theoretic capacity (670 mAh g^{-1}), non-toxic, low cost and easy synthesis. However, the intrinsical drawback of poor cycle performance restricts the practical application of CuO anode in lithium ion batteries [11–13]. It is well accepted that the morphology and size of CuO are important factors, which can greatly affect the electrochemical properties [14,15]. Hence, in the past few years, intensive research has focused on the shape control of CuO nanostructures to enhance the cyclability of CuO electrodes. For instance, Chen et al. reported the hydrothermal synthesis of dandelion-like CuO microspheres, and found that dandelion-like CuO electrodes delivered a reversible capacity more than 600 mAh g^{-1} up to 50 cycles [16]. Song et al. employed Cu_2O nanocubes as precursors to synthesize urchin-like CuO, which demonstrated an electrochemical capacity more than 560 mAh g^{-1} during 50 cycles [17]. Sheaf-like CuO, which exhibits a high rate capacity, was synthesized by Pan et al. [18]. Sun et al. demonstrated that CuO nanoribbons array electrode could deliver a reversible capacity as high as 608 mAh g^{-1} up to 275th cycle [19].

To date, various CuO nanostructures with improved electrochemical properties have been successfully synthesized. However, there should be still much space for progress with regard to the development of CuO anode materials, particularly in terms of novel morphology and controlled synthesis. The development of an economic pathway for controlled synthesis of CuO with different morphologies is critical for obtaining the optimal properties with respect to their potential applications. In the present work, we present the controlled synthesis of CuO nanostructures via a so-called composite-hydroxide-mediated approach [20]. The CuO with different morphologies such as nanosheets, nanowires and nanobundles is obtained. This approach consists of advantages of large-scale, easy control and without using any surfactant or template, which shows a perspective for controllable production of CuO nanostructures. The reaction processes and possible morphology transformation mechanism are discussed. In addition, as anode material for lithium ion batteries, the morphology-dependent electrochemical performances are also investigated.

2. Experimental

In a typical process, an amount of 20 g of mixed hydroxides (NaOH:KOH=51.5:48.5) was added into a Teflon vessel. The vessel was put in a furnace and heated up to 200 °C. After the

* Corresponding authors. Tel.: +86 29 82663034; fax: +86 29 82667872.
E-mail addresses: feiwang@mail.xjtu.edu.cn (F. Wang), xpsong@mail.xjtu.edu.cn (X. Song).
[1] Tel.: +86 29 82665892; fax: +86 29 82667872.

1386-9477/$ - see front matter © 2011 Elsevier B.V. All rights reserved.
doi:10.1016/j.physe.2011.09.030

hydroxides were totally molten, 0.34 g $CuCl_2 \cdot 2H_2O$ was added and the mixture was stirred by a Teflon bar until a uniform blue precursor was obtained. After that, the vessel was taken out and cooled to room temperature. A certain amount of the blue precursor was dissolved in various volumes of deionized water. After aging for several hours, the product was filtered and washed thoroughly by deionized water to remove residual hydroxides.

The crystal structures of the as-synthesized products were inspected by powder X-ray diffraction (Bruke D8-Advance) with Cu-Kα radiation (λ=0.15406 nm). The morphology and representative size of the products were observed with a field-emission scanning electron microscope (JEOS JSM-7000F).

Electrochemical performance of CuO nanostructures was investigated with two-electrode Swagelok cells. The working electrodes were prepared as follows: the mixture consisting of CuO, carbon black and binder polyvinylidene fluoride (PVDF) at a mass ratio of 80:10:10 was dispersed in N-methyl pyrrolidinone (NMP). Then, the slurry was coated uniformly onto a copper foil with a diameter of 10 mm and dried in vacuum at 100 °C. Test cells were assembled in argon filled glove box. Metallic lithium foil was used as counter electrode. The electrolyte was made of 1 M $LiPF_6$ dissolved in the mixture of ethylene carbonate (EC) and diethylene carbonate (DEC) with the volume ratio of 1:1. The galvanostatical charge and discharge tests were carried out on a battery testing system (Arbin BT2000) in the voltage range of 0.01 V–3.0 V (vs. Li/Li^+). Cyclic voltammograms were performed on Ametek VMC-4 electrochemical testing system between 3.0 V and 0 V at a scan rate of 0.5 mV s^{-1}.

3. Results and discussion

Fig. 1 displays the SEM images of the samples obtained by dissolving 0.2 g precursor in different volumes of 1 ml, 2 ml, 5 ml and 20 ml H_2O. The as-synthesized product obtained in 1 ml water reveals 3D hierarchical, flower-like morphology, which is randomly assembled by extremely thin nanosheets (Fig. 1a). The single nanosheet is spontaneously convolute, with the thickness likely less than 30 nm. When the volume of water is increased up to 5 ml, the morphology of 1D nanostructure is obtained. The major produces are nanowires (Fig. 1c), which are about 50 nm in diameter and several micrometers in length. Further increasing the water volume up to 20 ml, the nanobundles (Fig. 1d) constructed by nanorods instead of single nanowires are formed. Besides, the morphology of the coexistence of nanosheets and nanowires is obtained in 2 ml water (Fig. 1b). It is reasonable for the result of competition balance between the formation of nanosheet and nanowire.

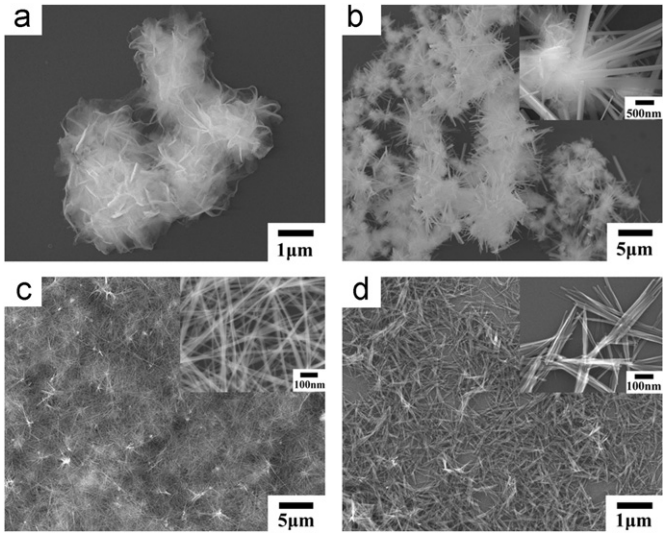

Fig. 1. SEM images of as-synthesized nanostructures obtained by dissolving 0.2 g precursor in different volumes of water: (a) 1 ml, (b) 2 ml, (c) 5 ml and (d) 20 ml.

Fig. 2 shows the XRD patterns of as-synthesized samples obtained in different volumes of water. The XRD pattern of nanosheets is revealed in Fig. 2A, which indicates that all the diffraction peaks can be indexed as monoclinic CuO (JCPDS 05-0661) with lattice constants a=4.688 Å, b=3.423 Å and c=5.132 Å. No other peaks for impurities are observed, which shows the good phase purity. The curves in Fig. 2C and D, which are similar, show the XRD patterns of nanowires and nanobundles, respectively. All the diffraction peaks correspond well with orthorhombic $Cu(OH)_2$ (JCPDS 13-0420). When 2 ml water is used, the XRD result (Fig. 2B) indicates that the CuO is dominant while a trace of $Cu(OH)_2$ is also found. In summary, Table 1 describes the correlation between the morphology, composition and the volume of water. CuO nanosheet is obtained in low volume of water. When the volume of water is increased, there is a trend for the formation of 1D $Cu(OH)_2$ nanostructures. Specially, the coexistence of CuO and $Cu(OH)_2$ nanostructures is obtained when 2 ml water is used.

Schematic illustration of the possible morphology transformation mechanism is presented in Fig. 3. Firstly, the cuprate precursor is obtained in molten hydroxides via the following reaction [21]:

$$Cu^{2+} + 4OH^- \rightarrow [Cu(OH)_4]^{2-} \quad (1)$$

When the precursor is dissolved in water, precipitates are formed possibly due to the decomposition of cuprate and subsequent

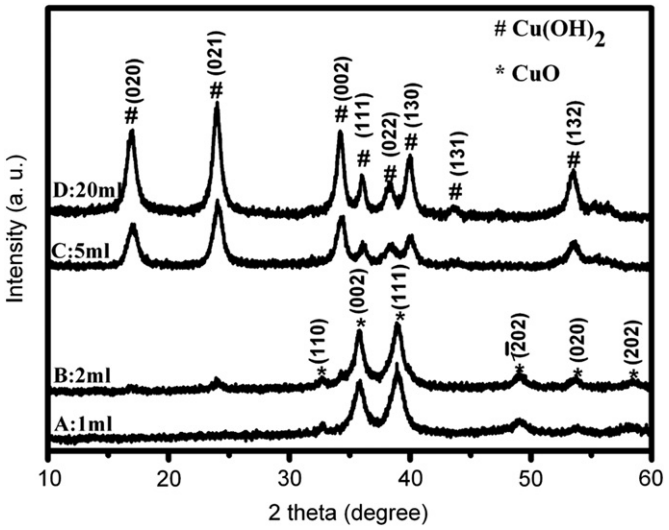

Fig. 2. XRD patterns of the samples obtained in different volumes of water.

Table 1
Summary of relationship between the morphology, composition and the volume of water.

Sample	Precursor (g)	H_2O (ml)	Aging time (h)	Morphology	Composition
A	0.2	1	6	nanosheet	CuO
B	0.2	2	6	nanosheet and nanowire	CuO and $Cu(OH)_2$
C	0.2	5	6	nanowire	$Cu(OH)_2$
D	0.2	20	6	nanobundle	$Cu(OH)_2$

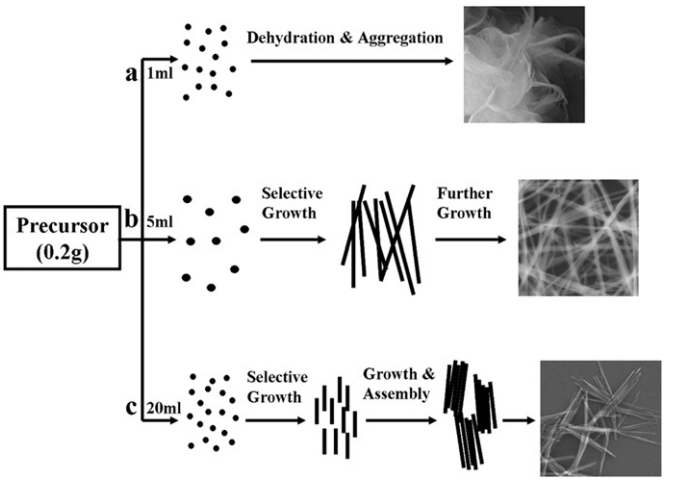

Fig. 3. Schematic illustration for the growth mechanism of CuO and $Cu(OH)_2$ nanostructures.

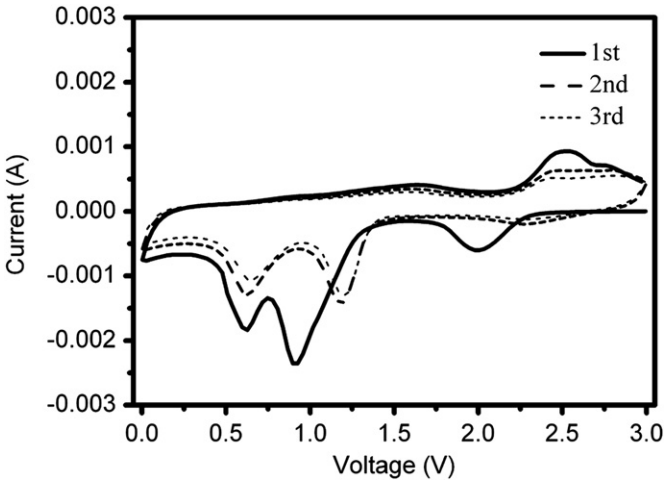

Fig. 4. First three CV curves for CuO nanosheet.

dehydration. The possible reactions involved in reaction process can be described as follows:

$$[Cu(OH)_4]^{2-} \rightarrow Cu(OH)_2\downarrow + 2OH^- \quad (2)$$

$$Cu(OH)_2 \rightarrow CuO + H_2O \quad (3)$$

Obviously, the concentration and pH value will affect the morphology transformation mechanism in aqueous solution. In this work, excessive hydroxides are used both as solvent and reactant. Actually, there are little hydroxides that would react with $CuCl_2 \cdot 2H_2O$ and most of the precursor consists of hydroxides. When 0.2 g precursor is dissolved in 1 ml, 2 ml, 5 ml and 20 ml, the pH value could be estimated to be 14.6, 14.3, 14 and 13.3, respectively. Finally, different concentrations of $[Cu(OH)_4]^{2-}$ and pH value result in the formation of various nanostructures. In fact, equation (3) occurs only in highly basic condition [22]. For the section of step a, high precursor concentration and large pH value are obtained when 0.2 g precursor is dissolved in 1 ml water. The CuO nanosheets are obtained due to the dehydration of $Cu(OH)_2$ and further aggregation. However, when 0.2 g precursor is dissolved in 5 ml water, Only $Cu(OH)_2$ can be obtained because the reaction (3) is restrained. $Cu(OH)_2$ is a layered material and easily forms 1D nanostructures with the orthorhombic phase due to the selective aggregation and assembly along the [1 0 0] direction [23,24]. Therefore, $Cu(OH)_2$ nanowires are formed as showed in step b. On the other hand, the further increase of water results in low basic condition (step c). A large drive force for reaction (2) is obtained and more nuclears are formed. The more nuclears as well as the lower concentration of $[Cu(OH)_4]^{2-}$ limit the growth of $Cu(OH)_2$ and result in the formation of nanorods. Finally, $Cu(OH)_2$ nanorods tend to form nanobundles, which should be ascribed to the decrease of surface energy.

To investigate the electrochemical properties of CuO nanostructures, CuO nanowires and nanobundles are obtained by heat-treating $Cu(OH)_2$ nanowires and nanobundles at 200 °C, respectively, while the as-prepared CuO nanosheets are used without further treatment. It is found that the morphologies of CuO nanowires and nanobundles are preserved after the heat treatment (Fig. 5 inset). The electrochemical reactions are investigated by cyclic voltammograms. Typically, Fig. 4 shows the CV curves of the CuO nanosheet at a scan rate of 0.5 mV s^{-1}. During the first cathodic scan, three peaks near 2.0 V, 0.9 V and 0.6 V could be observed. Compared to the initial cycle, a decrease of peak intensity and a shift of the potential to the positive direction are revealed in the subsequent cycles. These cathodic peaks correspond to a multistep electrochemical reaction, which is generally attributed to the solid–solution mechanism with formation of intermediate phase, the reductive reaction from CuO to Cu_2O and further decomposition to Cu and Li_2O [25,26]. Moreover, the cathodic peak at about 2.0 V is also ascribed to the formation of SEI during the first discharge process, the decomposition of electrolyte and the reactions of the adsorbed impurities on active material surfaces [27,28]. These reactions are usually irreversible and the peak near 2.0 V is absent in the subsequent cycles. In the anodic scans, one peak in the range of 2.3 V–2.7 V is recorded, which are ascribed to the partial formation of Cu_2O and the oxidation of Cu_2O to CuO.

Fig. 5 displays the first two discharge–charge curves and cycle performances for CuO nanosheets, nanowires and nanobundles. All the three electrodes exhibit similar discharge–charge behaviors and the discharge–charge plateaus are all corresponding well with the cathodic and anodic peaks in Fig. 4. However, the specific capacities of the three electrodes are different from each other. The CuO nanosheet, nanowire and nanobundle morphology exhibit first discharge capacity of 1198 mAh g^{-1}, 1031 mAh g^{-1} and 967 mAh g^{-1}, and first charge capacity of 752 mAh g^{-1}, 670 mAh g^{-1} and 671 mAh g^{-1}, respectively. Both the reversible capacities and irreversible capacities of nanosheet are higher than other two nanostructures. The differences can be attributed to the different morphologies of CuO, which greatly affect the surface areas of the electrodes. Usually, Li-driven formation of nanoscale Cu dispersed into Li_2O matrix goes with the reduction of electrolyte and the formation of SEI films in the first discharge process. It is irreversible and results in the decrease of capacity and low coulombic efficiency [29–31]. Hence, CuO nanosheet with 3D hierarchical morphology accommodates more surface areas for SEI films and shows the largest specific capacity and limited initial coulombic efficiency in the first cycle.

The cycle performances of CuO with different morphologies are shown in Fig. 5d. Obviously, the CuO nanosheet reveals higher reversible capacities and better capacity retention than those of CuO nanowires and nanobundles. A slow capacity fading could be found and a stable reversible capacity of more than 420 mAh g^{-1} is achieved after 40 cycles. For CuO nanowires and nanobundles, the reversible capacity is only 275 and 177 mAh g^{-1} after 40 cycles, respectively. As compared to the reported CuO nanowires, nanorods and many other 1D nanostructures [19,32], the as-synthesized CuO nanowires and nanobundles exhibit the poor cycle performance. The rapid loss of capacity may be due to the severe volume expansion and contraction during the lithiation/delithiation processes, which results in poor electrical contact and rapid deterioration in capacity. However, the CuO nanosheets exhibit the improved cycle performance. The hierarchical

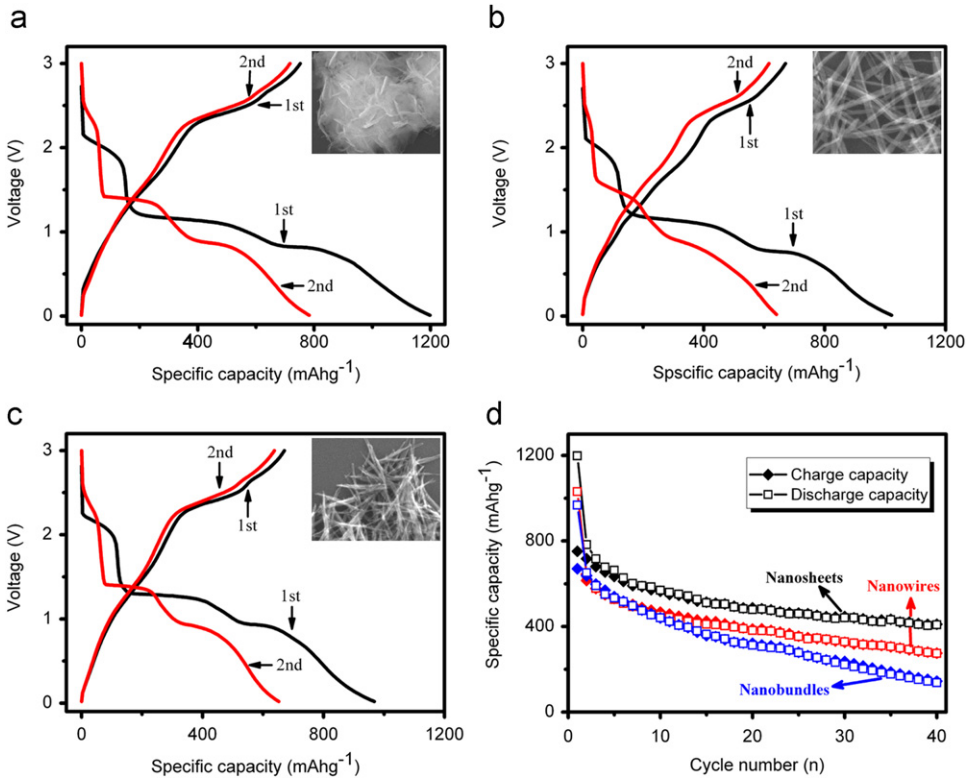

Fig. 5. First two discharge–charge curves for CuO nanostructures: (a) nanosheet, (b) nanowire, (c) nanobundle and (d) cycle performance of CuO nanostructures.

morphology of CuO nanosheet can relieve the stress associated with the drastic volume change and reduce the capacity fade. Hence, the morphology of CuO electrodes can greatly affect their electrochemical properties. The obtained CuO nanosheet shows good cycle stability, which is comparable to those of reported CuO nanostructures [14,15,33].

4. Conclusions

In summary, various CuO nanostructures with different morphologies, such as nanosheets, nanowires and nanobundles were synthesized via a composite-hydroxide-mediated route. The composition and the morphology can be easily tailored by adjusting the concentration and the pH value. As anode materials for lithium ion batteries, CuO nanosheets delivered a high reversible capacity of more than 420 mAh g^{-1} and a slow capacity fading up to 40 cycles, which showed better electrochemical performance than CuO nanowires and nanobundles.

Acknowledgments

This work was supported by National Natural Science Foundation of China (Grant nos. 51002117, 51071116, 51071117 and 50871081), Specialized Research Fund for the Doctoral Program of Higher Education of China (20100201120049) and Fundamental Research Funds for the Central Universities (0109-08143017, 08143029).

References

[1] X. Wang, C.G. Hua, H. Liu, G.J. Du, X.S. He, Y. Xi, Sensors and Actuators B: Chemical 144 (2010) 220.
[2] Y.M. Li, J. Liang, Z.L. Tao, J. Chen, Materials Research Bulletin 43 (2008) 2380.
[3] Y.S. Kim, I.S. Hwang, S.J. Kim, C.Y. Lee, J.H. Lee, Actuators B: Chemical 135 (2008) 298.
[4] X.G. Zheng, C.N. Xu, Y. Tomokiyo, E. Tanaka, H. Yamada, Y. Soejima, Physical Review Letters 85 (2000) 5170.
[5] C.T. Hsieh, J.M. Chen, H.H. Lin, H.C. Shih, Applied Physics Letters 83 (2003) 3383.
[6] Y.W. Zhu, T. Yu, F.C. Cheong, X.J. Xu, C.T. Lim, V.B.C. Tan, J.T.L. Thong, C.H. Sow, Nanotechnology 16 (2005) 88.
[7] L.P. Xu, S. Sithambaram, Y.S. Zhang, C.H. Chen, L. Jin, R. Joesten, S.L. Suib, Chemistry of Materials 21 (2009) 1253.
[8] J.Y. Kim, J.C. Park, H. Kang, H. Song, K.H. Park, Chemical Communications 46 (2010) 439.
[9] P. Poizot, S. Laruelle, S. Grugeon, L. Dupont, J.M. Tarascon, Nature 407 (2000) 496.
[10] H. Li, Z.X. Wang, L.Q. Chen, X.J. Huang, Advanced Materials 21 (2009) 4593.
[11] S.Y. Gao, S.X. Yang, J. Shu, S.X. Zhang, Z.D. Li, K. Jiang, Journal of Physical Chemistry C 112 (2008) 19324.
[12] S.F. Zheng, J.S. Hu, L.S. Zhong, W.G. Song, L.J. Wan, Y.G. Guo, Chemistry of Materials 20 (2008) 3617.
[13] B. Wang, X.L. Wu, C.Y. Shu, Y.G. Guo, C.R. Wang, Journal of Materials Chemistry 20 (2010) 10661.
[14] J.Y. Xiang, J.P. Tu, L. Zhang, Y. Zhou, X.L. Wang, S.J. Shi, Journal of Power Sources 195 (2010) 313.
[15] J.Y. Xiang, J.P. Tu, L. Zhang, Y. Zhou, X.L. Wang, S.J. Shi, Electrochimica Acta 55 (2010) 1820.
[16] S.Q. Wang, J.Y. Zhang, C.H. Chen, Scripta Materialia 57 (2007) 337.
[17] J.C. Park, J. Kim, H. Kwon, H. Song, Advanced Materials 20 (2008) 1.
[18] Q.T. Pan, K.H. Huang, S.B. Ni, F. Yang, S.M. Lin, D.Y. He, Journal of Alloys and Compounds 484 (2009) 322.
[19] F.S. Ke, L. Huang, G.Z. Wei, L.J. Xue, J.T. Li, B. Zhang, S.R. Chen, X.Y. Fan, S.G. Sun, Electrochimica Acta 54 (2009) 5825.
[20] C.G. Hu, Y. Xi, H. Liu, Z.L. Wang, Journal of Materials Chemistry 19 (2009) 858.
[21] Z.H. Yang, J. Xu, W.X. Zhang, A.P. Liu, S.P. Tang, Journal of Solid State Chemistry 180 (2007) 1390.
[22] X.F. Wu, H. Bai, J.X. Zhang, F.E. Chen, G.Q. Shi, Journal of Physical Chemistry B 109 (2005) 22836.
[23] X.G. Wen, W.X. Zhang, S.H. Yang, Nano Letters 2 (2002) 1397.
[24] G.H. Du, G.V. Tendeloo, Chemical Physics Letters 393 (2004) 64.
[25] A. Debart, L. Dupont, P. Poizot, J.B. Leriche, J.M. Tarascon, Journal of the Electrochemical Society 148 (2001) A1266.
[26] J.Y. Xiang, J.P. Tu, Y.Q. Qiao, X.L. Wang, J. Zhong, D. Zhang, C.D. Gu, Journal of Physical Chemistry C 115 (2011) 2505.
[27] P. Poizot, S. Laruelle, S. Grugeon, L. Dupont, J.-M. Tarascon, Journal of Power Sources 97/98 (2001) 235.

[28] Y.J. Mai, X.L. Wang, J.Y. Xiang, Y.Q. Qiao, D. Zhang, C.D. Gu, J.P. Tu, Electrochimica Acta 56 (2011) 2306.
[29] S. Laruelle, S. Grugeon, P. Poizot, M. Dolle, L. Dupont, J.M. Tarascon, Journal of the Electrochemical Society 149 (2002) A627.
[30] E.A. Souza, R. Landers, L.P. Cardoso, T.G.S. Cruz, M.H. Tabacniks, A. Gorenstein, Journal of Power Sources 155 (2006) 358.
[31] J.K. Feng, H. Xia, M.O. Lai, L. Lu, Materials Research Bulletin 46 (2011) 424.
[32] X.P. Gao, J.L. Bao, G.L. Pan, H.Y. Zhu, P.X. Huang, F. Wu, D.Y. Song, Journal of Physical Chemistry B 108 (2004) 5547.
[33] J.Y. Xiang, J.P. Tu, J. Zhang, J. Zhong, D. Zhang, J.P. Cheng, Electrochemistry Communications. 12 (2010) 1103.